The sensors for the intelligent micro washing system

Work report 6, 5-Feb-96
Geert Langereis

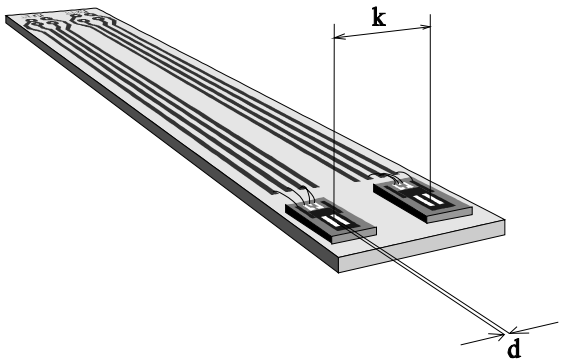

1. Introduction

In the preceding work report, a set of parameters was selected which will give a quite complete impression of washing processes. A list of sensors for determining these parameters was given as well. From this inventarisation, two major shortcomings in the available sensors became clear.
The first concerns the measurement of bleach activity. Amperometric detection appears to be the best method for determining bleaching agents. In practice this means that the concentration of bleaching agents is being measured by evoking an electrochemical reaction at an inert (noble) metal electrode which is being placed in the bulk solution. Because a lot of interfering species will be present in this bulk solution, the selectivity of the measurement will be a problem.
Secondly, no satisfying sensors for determining hardness or the calcium concentration were reported. A calcium ChemFET could be a candidate, but the use of lipophilic membranes in washing processes is not desired.
In the same report it was stated that the only way to make a reliable sensor system, which means a sensor with a decent reference system and without calibration problems, is to combine a sensor with an accurate actuator device. In this report, a sensor-actuator system is being evaluated which gives promising results for measuring hydrogen peroxide.

2. Bleaching

Bleaches are added to detergents to get a lighter shade in the colour of an object. Physically this implies increase of the reflectance of visible light at the expense of absorption. Chemical bleaching is the removal of non-washable soils by reductive or oxidative decomposition of chromophoric systems. The oxidative bleaches are more common in washing processes. In laundry, components are present that become colourless if they are bleached reductively and return to their coloured forms if they are oxidized by air [1].

In many countries outside Europe the most common bleaching component is sodium-hypochlorid. In Europe the dominant bleaches are active oxigen based. The active bleaching component is the intermediate hydrogen peroxide anion which is converted from hydrogen peroxide in alkaline medium.

The most important source for hydrogen peroxide is sodium perborate ($NaBO_3{}^{\backprime}4H_2O$) which is present in the crystalline form as the peroxodiborate ion. This ion has excellent dry life time and hydrolyses in water to hydrogen peroxide.

The peroxide is most active at 90°C, to wash at lower temperatures (<60°C) a bleach activator must be added. When present in wash liquor of pH 9-12, these activators react preferentially with hydrogen peroxide to form organic peroxy acids which have a higher oxidation potential than hydrogen peroxide. An example is TetraAcetyl-EthyleneDiamine (TAED).

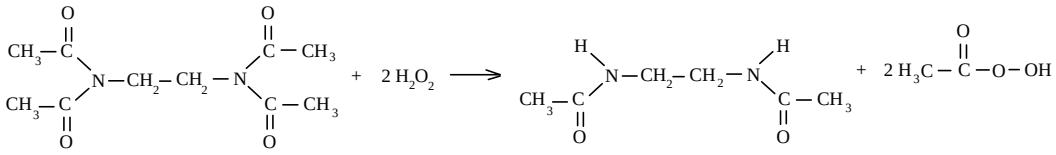

Figure 2.1: Reaction of TAED and hydrogen peroxide to peroxyacetic acid

The current approach is the lowering of bleaching temperature by bleaching catalysis where the bleaching power of sodium perborate is increased by some heavy metal chalates.

Because bleaches are oxidative components, most detection methods are amperometric. The problem with amperometric detection is that in a medium like washing liqour, a lot of interfering reactions can be expected.

One possability is to cover the sensor with a membrane to guarantee the necessary selectivity. However, this requires a more complicated technology for fabricating the sensor, and will increase the fragility of the device.

Another option is to perform the amperometric experiment in the conventional way, and to measure whether the desired electrode reaction was selected. This method will be explained in a following section.

3. Chemical properties of hydrogen peroxide

An elegant way to represent the reactions and equilibrium formulae is by making a Pourbaix diagram [2]. This diagram contains information on both the acid-base behaviour and electrochemical reactions plotted in a potential versus pH graph.

3.1. Acid base behaviour

Decomposition of hydrogen peroxide to the intermediate hydrogen peroxide anion satisfies:

$$H_2O_2 \Leftrightarrow HO_2^- + H^+ \qquad (3.1)$$

with the acid constant defined as:

$$k_a = \frac{[HO_2^-]\cdot[H^+]}{[H_2O_2]} = 2.4\cdot 10^{-12} \qquad (3.2)$$

from which it can be calculated that at pH = 10 the hydrogen peroxide is dissosiated for only 2.3%. Taking the logarithm of this k_a equation yields the first equation for the construction of the Pourbaix diagram:

$$\log\frac{[HO_2^-]}{[H_2O_2]} = -11.63 + \mathrm{pH}. \qquad (3.3)$$

It appears that for pH = 11.63 the ratio $[HO_2^-]/[H_2O_2] = 1$.

3.2. Electrochemical reactions

For both HO_2^- and H_2O_2 an electrochemical interaction with water and H^+ can be observed:

$$H_2O_2 + 2H^+ + 2e^- \Leftrightarrow 2H_2O \qquad E^0 = 1.776 \qquad (3.4a)$$

$$HO_2^- + 3H^+ + 2e^- \Leftrightarrow 2H_2O \qquad E^0 = 2.119 \qquad (3.5a)$$

which results in the following potential/concentration dependencies:

$$E^{0'} = 1.776 + \frac{RT}{2F\log(e)}\log[H_2O_2] - \frac{RT}{F\log(e)}pH \qquad (3.4b)$$

$$E^{0'} = 2.119 + \frac{RT}{2F\log(e)}\log[HO_2^-] - \frac{3RT}{2F\log(e)}pH. \qquad (3.5b)$$

The electrochemical reactions of HO_2^- and H_2O_2 with dissolved oxygen are:

$$O_2 + 2H^+ + 2e^- \Leftrightarrow H_2O_2 \qquad E^0 = 0.695 \qquad (3.6a)$$

$$HO_2^- \Leftrightarrow H^+ + O_2 + 2e^- \qquad E^0 = 0.338 \qquad (3.7a)$$

with the corresponding potential/concentration equations:

$$E^{0'} = 0.695 + \frac{RT}{2F\log(e)}\log\frac{pO_2}{[H_2O_2]} - \frac{RT}{F\log(e)}pH \qquad (3.6b)$$

$$E^{0'} = 0.338 + \frac{RT}{2F\log(e)}\log\frac{pO_2}{[HO_2^-]} - \frac{RT}{2F\log(e)}pH. \qquad (3.7b)$$

3.3. The Pourbaix diagram

When the equations (3.3), (3.4b), (3.5b), (3.6b) and (3.7b) are plotted in a single potential versus pH plot, assuming some values for the concentrations of O2, H_2O_2 and HO_2^-, this plot is referred to as Pourbaix diagram [2].

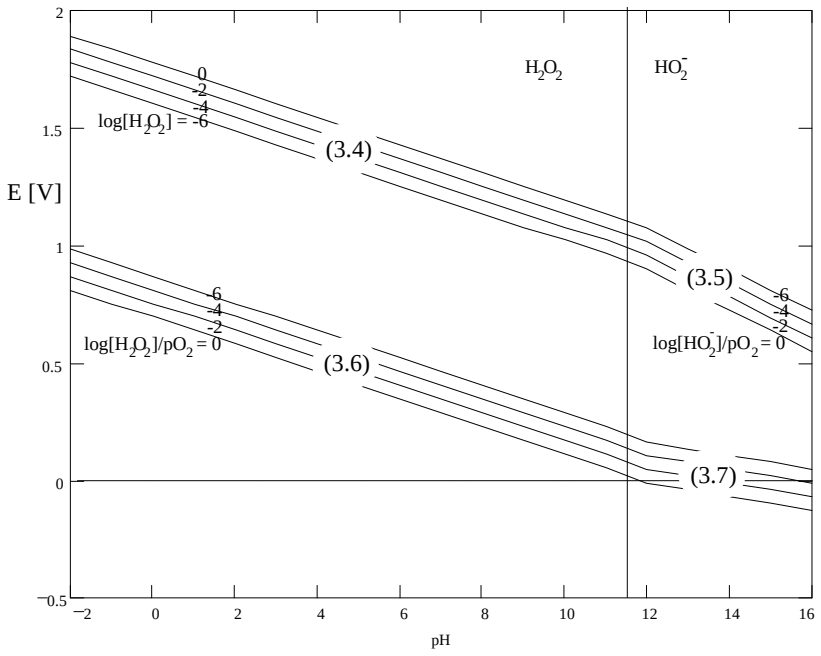

Fig. 3.1: The Pourbaix diagram for the system H_2O_2-water at 25°C

From this graph it can be concluded that below the lines of the equations (3.4) and (3.5), hydrogen peroxide can act as an oxidizing agent with the formation of water. Above the lines of the equations (3.6) and (3.7), hydrogen peroxide is a reducing agent with the formation of dissolved oxygen. These two domains have a common area, in which hydrogen peroxide is said to be double unstable and can decompose into water and oxygen.

$$\begin{array}{ll} H_2O_2 + 2H^+ + 2e^- & \Leftrightarrow H_2O \\ H_2O_2 & \Leftrightarrow O_2 + 2H^+ + 2e^- \\ \hline 2H_2O_2 & \Leftrightarrow 2H_2O + O_2 \end{array}$$

So at a metallic surface with an electrode potential in the range of double instability, the decomposition of hydrogen peroxide is being catalized. Because this decomposition process is much slower than electrochemical reactions involved with amperometric experiments, this phenomenon is not likely to be of interest during a measurement.

4. Chrono-amprometric detection

A chrono amperometric experiment consists of the application of a potential step to a chemically inert metal electrode in an electrolyte while monitoring the current. Under certain conditions the concentration of the reacting species can simply be evaluated from the measured response. Models for the current response are well-developed for various electrode shapes.

4.1. The Cottrell equation

At first instance a step is being considered from a value where no electrolysis occurs to a value in the mass-transfer-controlled region (diffusion only). Assume that the evoked reaction is represented by:

$$Ox + e^- \rightarrow Red \qquad (4.1)$$

and that a planar electrode is being used. The calculation of the diffusion limited current and the concentration profile $C_{Ox}(x,t)$ involves the solution of the linear diffusion equation:

$$\frac{\delta C_{Ox}(x,t)}{\delta t} = D_{Ox}\frac{\delta^2 C_{Ox}(x,t)}{\delta x^2} \qquad (4.2)$$

with D_{Ox} the diffusion coefficient of the oxidizing species. Three boundary conditions are assumed (C_{Ox}^* is the bulk concentration):

- $\lim_{x\to\infty} C_{Ox}(x,t) = C_{Ox}^*$ at x = ¥ the concentration is unaffected;
- $C_{Ox}(x,0) = C_{Ox}^*$ homogenity of the solution at t = 0;
- $C_{Ox}(0,t) = 0$ immediate, complete depletion of Ox at x = 0.

Under this conditions the diffusion equation gives the solution [3]:

$$i(t) = nFAC_{Ox}^*\sqrt{\frac{D_{Ox}}{\pi t}} \qquad (4.3)$$

with n the number of electrons transferred, F the Faraday constant, A the electrode surface C_{Ox}^* the bulk concentration and D_{Ox} the diffusion coefficient. This equation is known as the Cottrell equation and is interesting because the current response is not

a function of the potential step size. Notice that an i(t) versus 1/Öt plot will be a linear curve with a C_O^* dependent slope.
The expression for the concentration profile becomes:

$$C_{Ox}(x,t) = C_{Ox}^* \operatorname{erf}\left(\frac{x}{2\sqrt{D_{0x}t}}\right) \qquad (4.4)$$

with the x-axis perpendicular to the electrode surface.

From the third boundary condition an immediate and complete depletion of the oxidizing species at the electrode surface was assumed. When This is not the case, the extended Cottrell equation is valid:

$$i(t) = nFAC_{Ox}^*\sqrt{\frac{D_{Ox}}{\pi t}}\left[1+\sqrt{\frac{D_{Ox}}{D_{Red}}}e^{\frac{nF}{RT}(E-E^0)}\right]^{-1} \qquad (4.5)$$

which includes the step size E. The constant R is the gas constant, E^0 the redox potential for the reaction (4.1) and D_{Red} the diffusion coefficient for the reduced species.
When the (negative) step size E becomes large, the exponential term becomes zero and the extended Cottrell equation reduces to the normal Cottrell equation. The step size required to deplete the electrode surface immediately, which means to reduce equation (4.5) to (4.3), can be calculated from the ration between these equations:

$$a = \frac{1}{1+\sqrt{\frac{D_{Ox}}{D_{Red}}}e^{\frac{nF}{RT}(E-E^0)}}$$

where the constant a can bee seen as the accuracy. To have an accuracy of a·100%, the absolute value of the step size must be larger than:

$$|E| > \left|E^0 + \frac{RT}{nF}\ln\left(\sqrt{\frac{D_{Red}}{D_{Ox}}}\left(\frac{1}{a}-1\right)\right)\right| \qquad (4.6)$$

For example for the electrode reaction $Fe^{3+} + e^- \rightarrow Fe^{2+}$, the diffusion constants are:

$D_{Fe^{2+}} = 1.44\cdot10^{-9}$ m^2/s and

$D_{Fe^{3+}} = 1.81\cdot10^{-9}$ m^2/s

so for 95% accuracy the step size must be 78 mV larger than E^0.

4.2. Sampled current experiment

At various potential step sizes, four regions can be observed:

1. First, when the step size is smaller than E^0, no current will be measured.
2. For step sizes larger than E_0, but not sufficiently large to deplete the electrode immediately from oxidizing species, the extended Cottrell equation (4.5) can be used. The current response is a function of the potential step size.
3. In the third region, the condition of immediate deplition is met and the extended Cottrell equation reduces to the normal Cottrell equation (4.3).
4. When the step size is in the order of the E^0 for the oxidizing of water the current will increase rapidly. For t ® ¥ a net current will remain.

Using the diffusion constants and redox potential for the couple Fe^{3+}/Fe^{2+}, some Mathcad 4.0 simulations were performed. Figure 4.1 gives the current responses on four different potential step sizes.

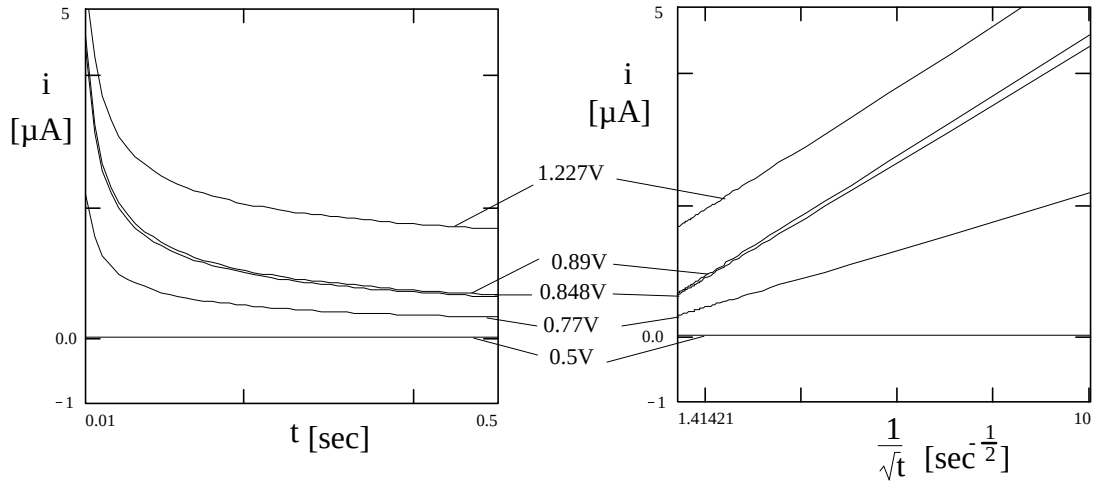

Fig. 4.1: Simulated chrono-amperometric experiments
[The same data is plotted in both an i(t) and an i(1/Öt) graph]

Because the redox potential for the couple Fe^{3+}/Fe^{2+} is 0.770 Volt, with a step size of E = 0.5 Volt no current is observed. The two curves where $E^0_{Fe} < E < E^0_{water}$ are almost identical because the criteria for Cottrell are met and the response is almost independent of the step size. The upper curve represents electrolysis of water and does not go to zero for t ® ¥.

This four-regions approach can be viewed when the current after time t is plotted as a function of the potential step size. Such a graph is referred to as a sampled current voltammogram. The time t must be chosen larger than the time necessary for capacative loading of the electrical double layer. From the same data as used for figure 4.1 a sampled current graph was made for t = 10 ms and t = 20 ms.

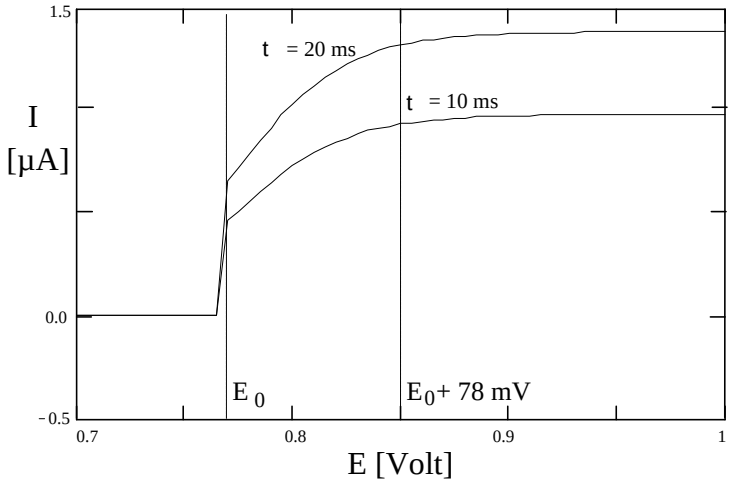

Fig. 4.2: A simulated sampled current experment

It can be concluded that for potential steps larger then about 0.9 volt, the response becomes independent of the step size and the Cottrell equation can be used. This is the region in which the chrono-amperometric experiment should be performed. The sampled current for steps in the range of the E^0 for electrolysis of water is not plotted. For 95% accuracy equation (4.6) showed that a step of E^0 + 78mV was required, this is in agreement with figure 4.2.

4.3. Some measurements using the Fe^{2+}/Fe^{3+} couple

In his 100 hours assignment, an Italian student Sergio Botti performed some measurements to verify the theory that was summarized in the previous subsections.

The measurement set-up
The experiments were carried out using a PAR 173 potentiostat and a PAR 276 controller, programmed with a personal computer. An Ag/AgCl reference electrode was used with a 0.5×1 cm^2 platinum reference electrode . The working electrode was a 1´2 mm^2 platinum thin-film on a silicon substrate mounted on a dip-stick. Because the understanding of the reaction mechanisms of hydrogen peroxide is very complicated, a more simple couple was evaluated. The reduction of Fe^{3+} to Fe^{2+} appeared to be a reaction without much interferences. The reaction of interest is:

$$Fe^{3+} + e^- \rightarrow Fe^{2+}, \qquad E^0 = 0.770V \qquad (4.7)$$

Sample solutions were used of 20, 10 and 1 mM $Fe(NO_3)_3$ in an acid environment created by HNO_3 acid. The solution was bubbled before each experiment using nitrogen gas.

Experimental

Figure 4.3 shows the sampled current voltammogram for the 10 mM solution. A sample time of t = 4 seconds was chosen.

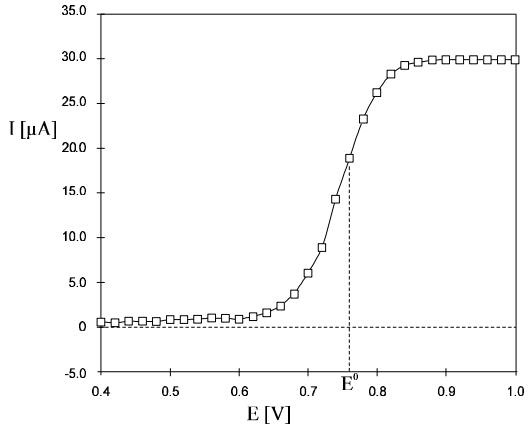

Fig. 4.3: Sampled current voltammogram for the reduction of Fe^{3+}

It can be seen that, in agreement with the calculations using equation (4.6), the current response becomes independent of the potential step size when $E > E^0 + 78$ mV.

A number of chronoamperometric experiments was performed with different potential steps and concentrations. As an example, the chrono amperometric plots for five different step sizes using a 20 mM solution are in figure 4.4.

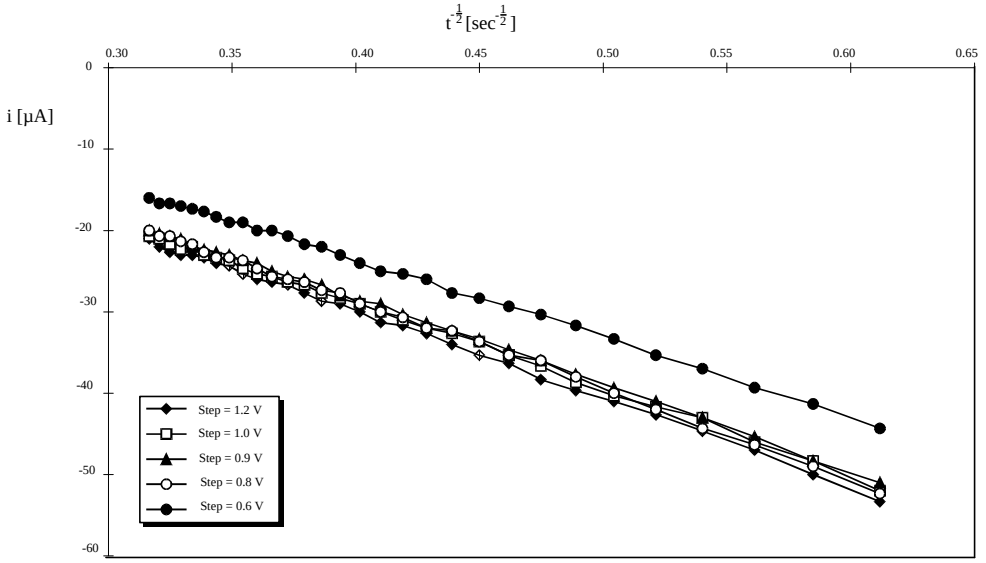

Fig. 4.4: Chrono amperometry for the reduction of 20 mM Fe^{3+}

One curve is included where the step size was not large enough, the other four show an almost step-size independent slope.

Results

Table 4.1 summarizes the results of the experiments. The data is being used for three different potential steps: 0.9, 1.0 and 1.2 Volt. Using the same concentration, the variation in measured slopes was very low (less then 5% of the average slope).

Table 4.1: Results of concentration detection using chrono-amperometry

Concentration [mM]	number of experiments	Average slope [A/sec^{½}]	Calculated conc. [mM]
20.0	3	$-1.1 \cdot 10^{-5}$	22
10.0	3	$-5.2 \cdot 10^{-6}$	11
1.00	3	$-7.0 \cdot 10^{-6}$	1.5

The fourth column gives the calculated concentrations. These are calculated from the Cottrell equation (4.3) using the average measured slope.

5. Feed-back by measuring the local pH

When the reaction:

$$H_2O_2 \rightarrow O_2 + 2H^+ + 2e^- \qquad E^0 = 0.695\ V \qquad (3.6a)$$

describes the dominant electrochemical behaviour, something interesting occurs. For each hydrogen peroxide molecule being oxidized, two H^+ ions are generated. This gives the possability of verifying an amperometric experiment by measuring the local pH. Instead of having a selective sensor, now a combined sensor-actuator system can be used which has the possability of qualifying the measurement.
The pH sensing can be done using either an ISFET or an iridium oxide potentiometric sensor. A possible set-up is drawn in figure 5.1.

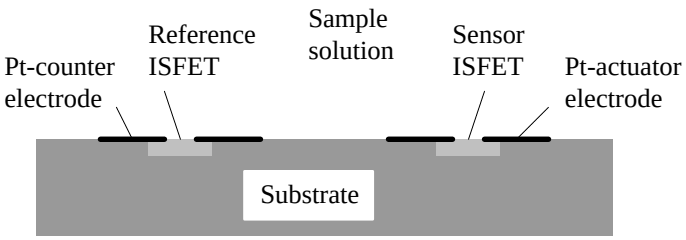

Fig. 5.1: Implementation of the combined sensor-actuator system

At first instance, only the Pt actuator electrode and an ideal pH sensing device is being considered. The model for the diffusion controlled H^+ response due to an chrono-amperometric experiment is derived in the following subsection.

5.1. Derivation of the theoretical behaviour

The calculation of diffusion controlled processes requires the solution of Fick's law:

$$\nabla^2 c = \frac{1}{D}\frac{\delta c}{\delta t} \qquad (5.1)$$

with D the diffusion coefficient and v the distribution which is a function of both the location (x,y,z) and time. From heat conduction theory a solution for this equation can be found. The response due to an instantaneous point source Q at (x_0, y_0, z_0) is given by [4]:

$$c_{point}(x,y,z,t) = \frac{Q}{\left(2\sqrt{\pi Dt}\right)^3} e^{-\frac{(x-x_0)^2+(y-y_0)^2+(z-z_0)^2}{4Dt}} \qquad (5.2)$$

and it can be seen that, when t ® 0, the value for c becomes zero at all point except for (x_0, y_0, z_0) where it becomes infinite. The integral

$$\int_{-\infty}^{\infty}\int_{-\infty}^{\infty}\int_{-\infty}^{\infty} c\,dx\,dy\,dz = Q \qquad (5.3)$$

for each t > 0. This affirms that the produced amount Q is not lost. For the two dimensional case, or when an instantaneous line source is being considered, equation (5.2) reduces to:

$$c_{line}(x,y,t) = \frac{Q}{4\pi Dt} e^{-\frac{(x-x_0)^2+(y-y_0)^2}{4Dt}}. \qquad (5.4)$$

Now consider a source of the structure shown in figure 5.2. The actuator plane consists of source points (x_0, y_0), the point of measurement is (x,y).

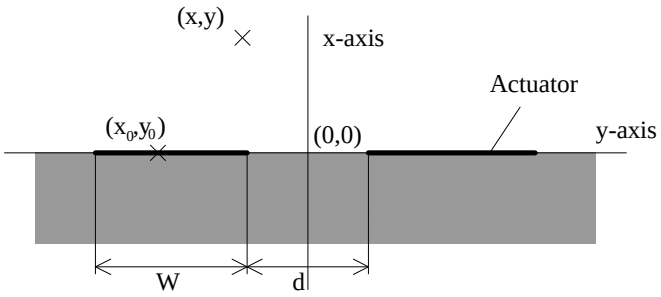

Fig 5.2: Source structure used for the mdelling

The actuator is a pair of strips with width w at a distance d. The origin is in the middle between these electrodes. Solution of the measured response at (x,y) due to an instantaneous amount Q produced at the electrodes at t = 0 follows from integration of (5.4) along the actuator:

$$c_{actuator}(x,y,t) = \int_{-\frac{d}{2}-w}^{-\frac{d}{2}} c_{line}(x,y,t)\,dy_0 + \int_{\frac{d}{2}}^{\frac{d}{2}+w} c_{line}(x,y,t)\,dy_0. \qquad (5.5)$$

In this subsection only the method and the result is given while in appendix A a complete evaluation is given.

The next step is the calculation of the response due to a source which is not instantaneous, but satisfies the Cottrell equation (4.3). Now the constant Q is exchanged by a sequence of temporary sources dQ/dt (which is the current i through the actuator!) and the response can be found by convolution in time:

$$c(x,y,t) = \int_0^t i(\tau) \cdot c_{actuator}(x,y,t-\tau)d\tau \qquad (5.6)$$

where the term Q in $v_{actuator}$ must be set to 1. In appendix A this integral is being calculated for infinite width w at the point (0,0):

$$c(t) = \frac{1}{2} nFAC^*_{H_2O_2} \sqrt{\frac{D_{H_2O_2}}{D_{H^+}}} \left[1 - \frac{1}{\pi} \int_0^t \frac{\operatorname{erf}\left(\frac{d}{4\sqrt{(t-\tau)D_{H^+}}} \right)}{\sqrt{(t-\tau)\tau}} d\tau \right] \qquad (5.7)$$

with n the number of electrons transferred, F the Faraday constant, A the electrode surface, $C_{H2O2}{}^*$ the bulk concentration, D_{H^+} and D_{H2O2} the diffusion coefficients and d the distance between the electrodes. No closed form solution for the integral was found.

5.2. Understanding and simplifying the model

The exact solution of the diffusion equation is a rather complicated expression which can be understood and simplified by splitting the response into three regions in time. Using a normalized version of equation (5.7) and assuming $d/4\sqrt{D_{H^+}} = 1$, two plots were made.

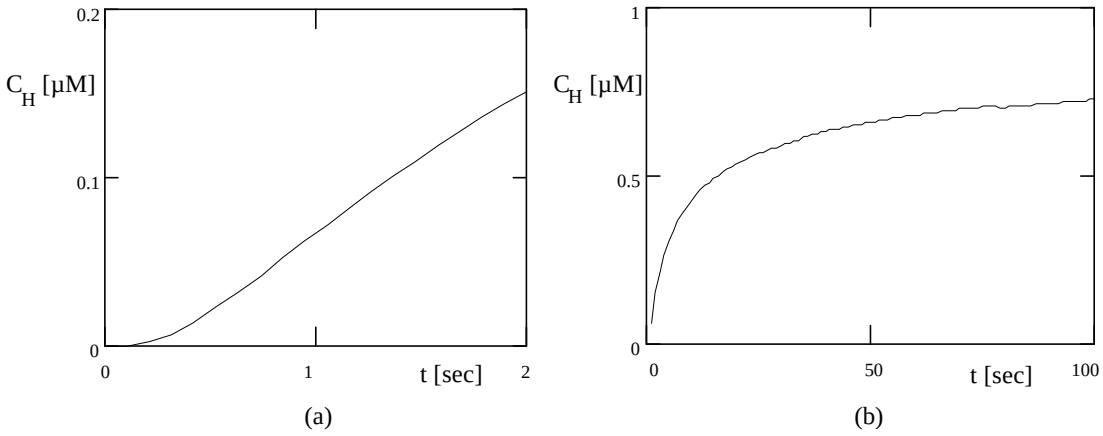

Fig. 5.3: Normalized simulation of the proton concentration during the first few seconds (a) and after some time (b)

In the first few seconds, the response will be around zero (figure 5.3a) because of the diffusion time necessary for mass transport from the working electrode to the sensor. The second region is the intermediate period, where the concentration rises (figure 2.3b) to the final concentration, which is the third region.

The exact solution (5.7) will be evaluated here for two cases. First a condition will be derived for the delay time as visualized in figure 5.3a, and after that the final H^+ concentration will be calculated.

Diffusion from the electrode to point of measurement
In the first moments after starting the chrono-amperometric experiment, the products of the electrochemical changes in the solution can not be sensed at the point of measurement (x,y) = (0,0). The generated H^+ ions must be transorted to the sensor by diffusion.
An expression for this dead-time can be obtained by drawing a straight line in figure 5.3a. A gentle choice is to take the point where the first derivative has it's maximum, as drawn in figure 5.4.

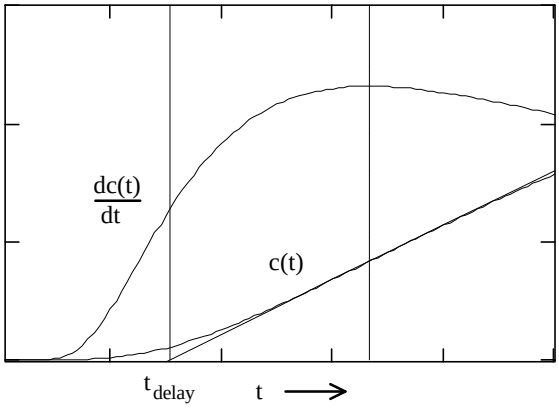

Fig. 5.4: Obtaining an impression for the delay time

In appendix A, an expression for the delay time is derived. This delay time is only a function of the electrode gap d and the diffusion constant of protons:

$$t_{delay} = \left[\sqrt{\pi}\left(\operatorname{erf}\sqrt{\frac{3}{2}} - 1 \right)\left(\frac{2}{3}\right)^{\frac{3}{2}} e^{\frac{3}{2}} + \frac{2}{3} \right]\left(\frac{d}{4\sqrt{D_{H^+}}} \right)^2 \qquad (5.8)$$

where the constant factor is about 0.307. When the substitution

$$L = \frac{d}{4\sqrt{D_{H^+}}} \qquad (5.9)$$

is made, it can be said that $t_{delay} \approx 0.307 L^2$.

Final concentration
It can be calcutated that for a large time t, the integral:

$$\lim_{t\to\infty}\int_0^t \frac{\operatorname{erf}\left(\frac{L}{\sqrt{(t-\tau)}}\right)}{\sqrt{(t-\tau)\tau}}\,d\tau = 0$$

so equation (5.7) becomes for t ® ¥:

$$C_{t\,inf} = \frac{1}{2} nFAC^*_{H_2O_2}\sqrt{\frac{D_{H_2O_2}}{D_{H^+}}}. \qquad (5.10)$$

where C_{tinf} is the local concentration of H^+ for t is infinity. From the series expansion of equation (5.7) as given in appendix A, it appears that for large t the ratio L^2/t determines the behaviour completely. So the deviation at time t from the final concentration C_{tinf} can be plotted normalized as in figure 5.5.

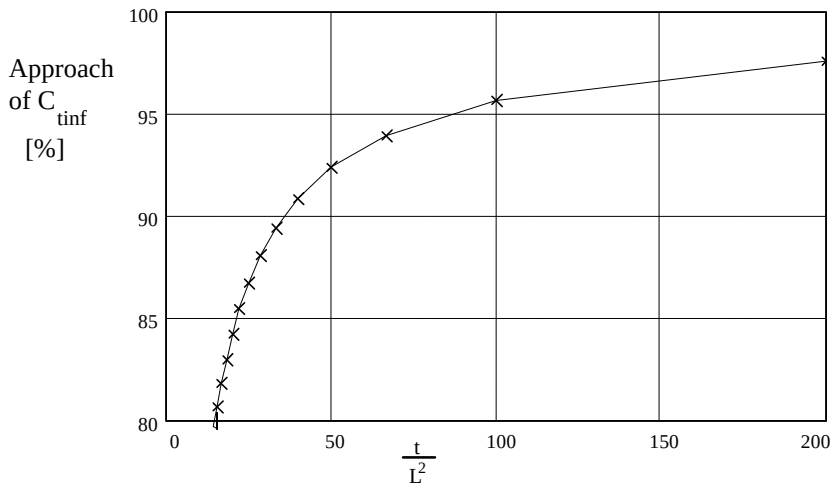

Fig 5.5: Accuracy of normalized configuration

For example, from this graph it appeares that when t > 100×L^2 the final concentration C_{tinf} is approached for 96%

5.3. Summary of the model

In the equation for the final H^+ concentration (5.10), the slope of the Cottrell equation

$$S = nFAC^*_{H_2O_2}\sqrt{\frac{D_{H_2O_2}}{\pi}} \qquad (5.11)$$

can be substituted. This results in the simple equation

$$C_{t\,inf} = \sqrt{\frac{\pi}{4D_{H^+}}} \cdot S. \qquad (5.12)$$

When the substitution

$$L = \frac{d}{4\sqrt{D_{H^+}}} \qquad (5.9)$$

is also used, all important equations can be written in terms of L, S and D_{H^+}. Table 5.1 gives both the models for the chono amperometric current and the resulting H^+ concentration.

Table 5.1: Summary of the model for chrono amperometry with monitored H^+ concentration

Period	H^+ Concentration at (0,0)	Measured current
$t < 0.307 \cdot L^2$	0	Capacitive
$0.307 \cdot L^2 > t > 100 \cdot L^2$	$\frac{\pi S}{2\sqrt{D_{H^+}}}\left(1 - \frac{1}{\pi}\int_0^t \frac{\mathrm{erf}\left(\frac{L}{\sqrt{(t-\tau)}}\right)}{\sqrt{(t-\tau)\tau}} d\tau\right)$	$\frac{S}{\sqrt{t}}$
$t > 100 \cdot L^2$	$C_{t\,inf} = \frac{\pi}{2\sqrt{D_{H^+}}} \cdot S$	≈ 0

The current follows from the chrono amperometric experiment. Just after the application of the potential step, the current will not be determined by the Cottrell equation but is controlled by capacitive loading of the electrical double layer of the working electrode. After $t > 100 \cdot L^2$ the current will be more then 10 times smaller then the current at $t = L^2$ and reduces to zero.

Table 5.2: typical values for the constants

actuator distance d [µm]	constant L [$sec^{½}$]	delay time t_{delay} [sec]	95 % rise time $t_{95\%}$ [sec]
40	0.10	$1.02 \cdot 10^{-5}$	$3.3 \cdot 10^{-3}$
120	0.31	$29.6 \cdot 10^{-3}$	9.6

A typical value for the constant L can be calculated using $D_{H^+} = 9.33 \cdot 10^{-9}$ m^2/s. This results in the values for L as given in table 5.2 from which the delay times can be calculated. The time after which C_{tinf} is given in the fourth column. Because the diffusion constant of H_2O_2 can not easily be found in literature, equal diffusion

constants for reducing and oxidizing species are assumed. A typical value for C_{tinf} at a H_2O_2 concentration of 1 mM and using an electrode area of two times 1×2 mm^2 is 1.2 mM. This means that due to a chronoamperometric experiment in a solution of pH 7, the local pH changes to 2.9 in $t_{95\%}$ seconds, independent of the potential step size.

5.4. Measurements

The measurement set-up
Electrochemical experiments are generally carried out using a potentiostat. In combination with an ISFET amplifier however, a grounding problem occurs. A schematic view of a potentiostat is drawn in figure 5.6 [3].

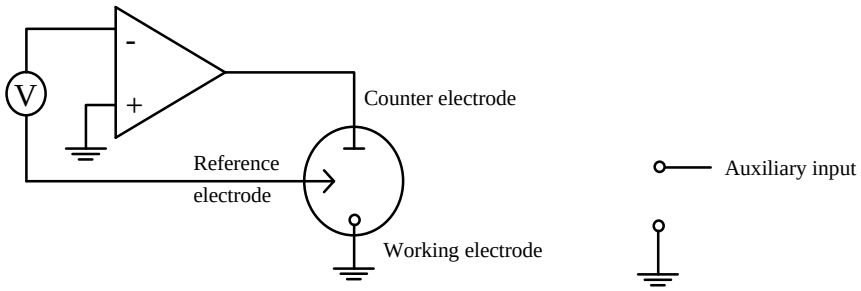

Fig. 5.6: Schematic set-up of a potentiostat with auxiliary input

In a normal potentiostat, the working electrode is grounded. Furthermore, the auxiliary input which is used to sample the ISFET response is relative to the ground. So, when a normal ISFET amplifier set-up is used, where the output is relative to the reference electrode (figure 5.7), a conflict appears because the reference electrode should be grounded now.

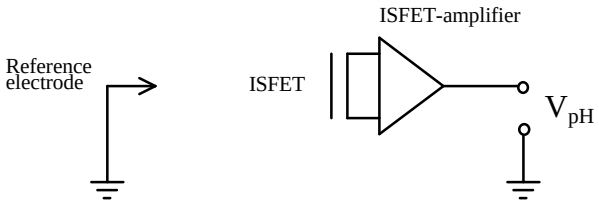

Fig. 5.7: ISFET amplifier set-up

This problem will not be solved when a floating ISFET amplifier is used: the potentiostat input potential V is still placed between the (virtual) ground and the reference electrode.
When using a differential ISFET set-up, however, the input potential V becomes a common signal and will not appear in the output signal.

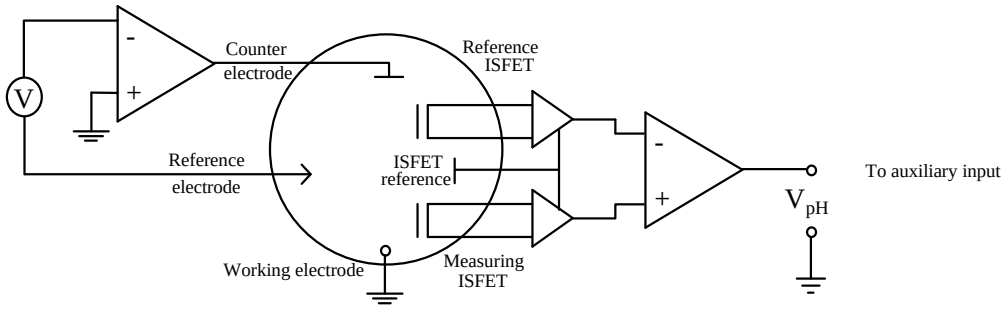

Fig. 5.8: Measurement set-up

The experiments were performed using a PAR 263A potentiostat with a PAR Model 270/250 computer control program. Two custom made ISFET amplifiers were used in combination with a standard differential amplifier.
For the actuator, the measuring ISFET and the reference ISFET a dipstick was used with two actuator ISFETs. The ISFETs were of type JH/GL date 10/95 with a 20/300 nm Ti/Pt actuator on a 30 nm Ta_2O_5 layer. The gap in the actuator (where the ISFET gate is located) had a width of d = 120 µm.

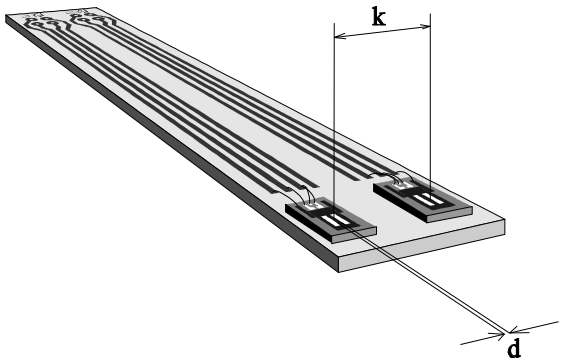

Fig. 5.9: The dipstick with two actuators/ISFET structures

The distance between the two ISFETs was k = 1 cm. Both the ISFET refererence and counter electrode where platinum electrodes of 0.5×1 cm^2, an Ag/AgCl reference electrode was used.

Experimental
The experiments were carried out in 10, 50 and 100 mM H_2O_2 solutions using KNO_3 as a background electrolyte. The pH of this solution was measured with a normal pH meter before each measurement.
Using the set-up of figure 5.8 a potential step of 1 volt was examined. Figure 5.10 gives both the actuator currents and the ISFET responses.

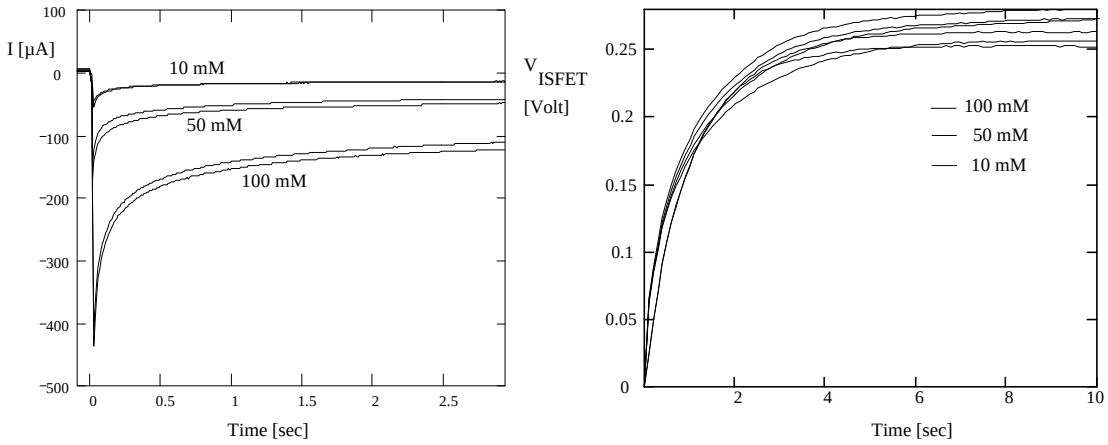

Fig 5.10: Measurements in 10, 50 and 100 mM H_2O_2 samples

The effect of diffusion from actuator to the sensor is visualized in figure 5.11 where the H^+ concentration is calculated from the ISFET potentials using the bulk pH and the potential at t = 0.

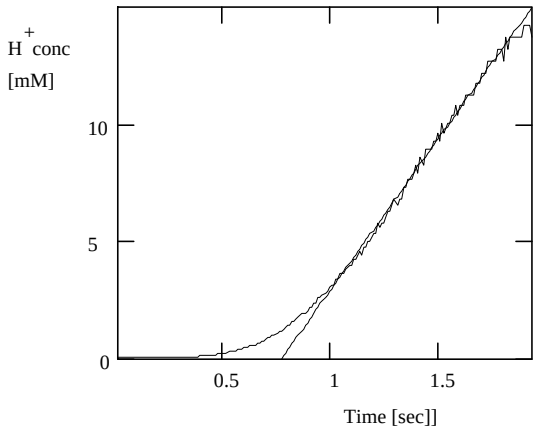

Fig 5.11: plot of the first few seconds of the response

Discussion

After some time the pH reaches a maximum value, which indicates a constant H^+ concentration. This rise time (which is about 10 seconds) is in agreement with the prediction in table 5.2.

In table 5.3 the data of figure 5.10 is evaluated. The first colomn contains the imposed concentration of the solution, column 2 the measured bulk pH.
The slope of the I versus $1/\sqrt{t}$ characteristic as theoretically given by equation (5.11) can be determined from the measured current response. The third column of table 5.3 summarizes the measured values. This satisfies the Cottrell equation because this slope is linear dependent on the concentration. Using n = 2, F = $9.6487 \cdot 10^4$ C/mol and A = 4 mm^2 a value for the diffusion coefficient of H_2O_2 can be calculated by comparing the measured slope to the theoretical one:

$$D_{H2O2} = 4.1 \cdot 10^{-6}\ m^2/s\ (\pm 1.5 \cdot 10^{-6}\ m^2/s)$$

Table 5.3: Evaluation of the time-current measurements

Conc [mM]	Measured bulk pH	Measured slopes of the I versus $1/\sqrt{t}$ relation [A/sec^2]	Calculated C_{tinf} from column 2 [M]	Equivalent pH change	Calculated ΔV in ISFET output [mV]	Measured ΔV in ISFET output [mV]
10	5.52	$1.052 \cdot 10^{-5}$	0.097	-4.51	266	250
		$1.105 \cdot 10^{-5}$	0.101	-4.53	267	262
50	5.20	$3.086 \cdot 10^{-5}$	0.283	-4.65	274	255
		$3.796 \cdot 10^{-5}$	0.348	-4.73	280	272
100	5.00	$7.931 \cdot 10^{-5}$	0.728	-4.86	287	273
		$8.610 \cdot 10^{-5}$	0.79	-4.90	289	282

This value is not necessary for determining the final H^+ concentration C_{tinf} because equation (5.12) gives the relation in terms of the slope S. The fourth column of table 5.3 gives the C_{tinf} values calculated from these slopes.
For finding the equivalent pH change that will be monitored with the ISFETs, the absolute bulk pH is necessary:

$$\Delta \mathrm{pH} = -\log\left(10^{-\mathrm{pH_{bulk}}} + C_{t\,inf}\right) - \mathrm{pH_{bulk}}.$$

This results in an ISFET amplifier output change of $\Delta \mathrm{pH} \cdot 59\mathrm{mV}$, given in colomn 6. The measured response does not change a lot with the concentration because it is the logarithm of a concentration. So it is not accurate to make a quantitative conclusion from the output potential. The measured output potentials are in global agreement with the measured ones (the last column).

From figure 5.11 the delay time appears to be 0.7 seconds, which is much larger then the calculated 30 ms. Probably, the assumption of an infinite large actuator is not right for the used configuration. A smaller hole in the actuator might solve the problem.

6. Conclusions

The development of this system was stopped because it does not fit in the idea of metal film-only sensors which was concluded in the previous work report.

During a chrono-amperometric experiment, the only way to control the selectivity is to vary the applied potential step. Which reactions take place is dependent on the electrochemical properties of the solution.
By monitoring the pH during a chrono-amperometric experiment, a decision can be made whether the experiment resulted in oxidizing hydrogen peroxide or not. So while the selectivity of this method is still poor, a feedback is now obtained on the result of the experiment.
For quantitative evaluations about the bulk hydrogen peroxide concentration, the response of the current is more accurate than making a conclusion from the ISFET potential change. This is because the last one requires the use of an anti-logarithmic operation.
The dimensions of the used actuator did not represent the model quite well: the actuator was not infinite large. This probably caused an error in the first part of the response which can be minimized by taking an actuator with a smaller gap for the sensor. When this part works, the diffusion coefficient of hydrogen peroxide can be measured.

The system described here is an example of the combination of existing sensors and actuators which results in more parameters then using the single sensors. Besides that the fundamental reference electrode problem which occurs when a potentiostat is used in combination with an ISFET amplifier is solved by taking a differential ISFET set-up.

Appendix A: Derivation of the diffusion model

In this appendix some derivations of equations used in chapter 5 are given.

*Equation (*5.*7):*
Derivation of the exact solution for the configuration of figure 5.*2 with w ® ¥*

The special solution for Fick's law:

$$\nabla^2 c = \frac{1}{D}\frac{\delta c}{\delta t} \tag{5.1}$$

for an instantaneous heat pulse at time t = 0 at point (x_0, y_0, z_0) is taken from Carslaw and Jeager [4]:

$$c_{\text{po int}}(x,y,z,t) = \frac{Q}{\left(2\sqrt{\pi Dt}\right)^3} e^{-\frac{(x-x_0)^2+(y-y_0)^2+(z-z_0)^2}{4Dt}} \tag{5.2}$$

When we are only interested in the two dimensional case (is equal to spatial integration over an infinite number of sources at (x_0,y_0,z_0) along the z axis):

$$\begin{aligned}
c_{\text{line}}(x,y,t) &= \int_{-\infty}^{\infty} c_{\text{po int}}(x,y,z,t)\,dz_0 \\
&= \int_{-\infty}^{\infty} \frac{Q}{\left(2\sqrt{\pi Dt}\right)^3} e^{-\frac{(x-x_0)^2+(y-y_0)^2+(z-z_0)^2}{4Dt}}\,dz_0 \\
&= \frac{Q}{\left(2\sqrt{\pi Dt}\right)^3} e^{-\frac{(x-x_0)^2+(y-y_0)^2}{4Dt}} \int_{-\infty}^{\infty} e^{-\frac{(z-z_0)^2}{4Dt}}\,dz_0 \\
&= \frac{Q}{\left(2\sqrt{\pi Dt}\right)^3} e^{-\frac{(x-x_0)^2+(y-y_0)^2}{4Dt}} \left[\sqrt{\pi Dt}\cdot \operatorname{erf}\left(\frac{z-z_0}{\sqrt{4Dt}}\right)\right]_{-\infty}^{\infty} \\
&= \frac{Q}{\left(2\sqrt{\pi Dt}\right)^3} e^{-\frac{(x-x_0)^2+(y-y_0)^2}{4Dt}} \left[\sqrt{\pi Dt} - -\sqrt{\pi Dt}\right]
\end{aligned}$$

$$c_{\text{line}}(x,y,t) = \frac{Q}{4\pi Dt} e^{-\frac{(x-x_0)^2+(y-y_0)^2}{4Dt}} \tag{5.4}$$

Now all the sources along the y-axis are being integrated along the structure:

$$c_{act}(x,y,t) = \int_{-\frac{d}{2}-w}^{-\frac{d}{2}} c_{line}(x,y,t)dy_0 + \int_{\frac{d}{2}}^{\frac{d}{2}+w} c_{line}(x,y,t)dy_0 \qquad (5.5)$$

$$c_{act}(x,y,t) = \int_{-\frac{d}{2}-w}^{-\frac{d}{2}} \frac{Q}{4\pi Dt} e^{-\frac{(x-x_0)^2+(y-y_0)^2}{4Dt}} dy_0 + \int_{\frac{d}{2}}^{\frac{d}{2}+w} \frac{Q}{4\pi Dt} e^{-\frac{(x-x_0)^2+(y-y_0)^2}{4Dt}} dy_0$$

$$= \frac{Q}{4\pi Dt} e^{-\frac{(x-x_0)^2}{4Dt}} \left(\int_{-\frac{d}{2}-w}^{-\frac{d}{2}} e^{-\frac{(y-y_0)^2}{4Dt}} dy_0 + \int_{\frac{d}{2}}^{\frac{d}{2}+w} e^{-\frac{(y-y_0)^2}{4Dt}} dy_0 \right)$$

The two integrals can be solved:

$$\int_{-\frac{d}{2}-w}^{-\frac{d}{2}} e^{-\frac{(y-y_0)^2}{4Dt}} dy_0 = \left[-\sqrt{\pi Dt} \cdot \mathrm{erf}\left(\frac{y-y_0}{\sqrt{4Dt}} \right) \right]_{-\frac{d}{2}-w}^{-\frac{d}{2}}$$

$$\int_{\frac{d}{2}}^{\frac{d}{2}+w} e^{-\frac{(y-y_0)^2}{4Dt}} dy_0 = \left[-\sqrt{\pi Dt} \cdot \mathrm{erf}\left(\frac{y-y_0}{\sqrt{4Dt}} \right) \right]_{\frac{d}{2}}^{\frac{d}{2}+w}$$

and the general solution becomes:

$$c_{act}(x,y,t) = \frac{-Q}{4\sqrt{\pi Dt}} e^{-\frac{(x-x_0)^2}{4Dt}} \left(\begin{array}{l} \mathrm{erf}\left(\frac{y+\frac{d}{2}}{\sqrt{4Dt}} \right) - \mathrm{erf}\left(\frac{y+\frac{d}{2}+w}{\sqrt{4Dt}} \right) \\ +\mathrm{erf}\left(\frac{y-\frac{d}{2}-w}{\sqrt{4Dt}} \right) - \mathrm{erf}\left(\frac{y-\frac{d}{2}}{\sqrt{4Dt}} \right) \end{array} \right)$$

When w ® ¥ two of the four error functions go to a constant value and assume x_0=0:

$$c_{act}(x,y,t) = \frac{Q}{4\sqrt{\pi Dt}} e^{-\frac{x^2}{4Dt}} \left(2 - \mathrm{erf}\left(\frac{y+\frac{d}{2}}{\sqrt{4Dt}} \right) + \mathrm{erf}\left(\frac{y-\frac{d}{2}}{\sqrt{4Dt}} \right) \right)$$

After integration in space, integration in time is performed. Now, the instantaneous point source Q is being exchanged by an infinite number of momentary sources dQ/dt. The value of this momentary source at tiome t is equal to the input current i(t). This momentary current is being integrated with a time-translated response function:

$$c(x,y,t) = \int_0^t i(\tau) \cdot c_{act}(x,y,t-\tau) d\tau \qquad (5.6)$$

and this special type of integral is referred to as convolution integral. Calculation using the Cottrell equation (4.3) yields:

$$c(x,y,t) = \int_0^t \frac{i(\tau)}{4\sqrt{\pi D_{H^+}(t-\tau)}} e^{-\frac{x^2}{4D_{H^+}(t-\tau)}} \left(2 - \operatorname{erf}\left(\frac{y+\frac{d}{2}}{\sqrt{4D_{H^+}(t-\tau)}}\right) + \operatorname{erf}\left(\frac{y-\frac{d}{2}}{\sqrt{4D_{H^+}(t-\tau)}}\right)\right) d\tau$$

$$= \int_0^t \frac{nFAC^*_{H_2O_2}\sqrt{\frac{D_{H_2O_2}}{\pi\tau}}}{4\sqrt{\pi D_{H^+}(t-\tau)}} e^{-\frac{x^2}{4D_{H^+}(t-\tau)}} \left(2 - \operatorname{erf}\left(\frac{y+\frac{d}{2}}{\sqrt{4D_{H^+}(t-\tau)}}\right) + \operatorname{erf}\left(\frac{y-\frac{d}{2}}{\sqrt{4D_{H^+}(t-\tau)}}\right)\right) d\tau$$

$$= \frac{nFAC^*_{H_2O_2}}{4\pi}\sqrt{\frac{D_{H_2O_2}}{D_{H^+}}} \int_0^t \frac{e^{-\frac{x^2}{4D_{H^+}(t-\tau)}}}{\sqrt{\tau(t-\tau)}} \left(2 - \operatorname{erf}\left(\frac{y+\frac{d}{2}}{\sqrt{4D_{H^+}(t-\tau)}}\right) + \operatorname{erf}\left(\frac{y-\frac{d}{2}}{\sqrt{4D_{H^+}(t-\tau)}}\right)\right) d\tau$$

At the location of the sensor (x,y) = (0,0) this simplifies to:

$$c(t) = \frac{nFAC^*_{H_2O_2}}{4\pi}\sqrt{\frac{D_{H_2O_2}}{D_{H^+}}} \int_0^t \frac{1}{\sqrt{\tau(t-\tau)}} \left(2 - 2\cdot\operatorname{erf}\left(\frac{d}{4\sqrt{D_{H^+}(t-\tau)}}\right)\right) d\tau$$

$$= \frac{nFAC^*_{H_2O_2}}{2\pi}\sqrt{\frac{D_{H_2O_2}}{D_{H^+}}} \left(\int_0^t \frac{1}{\sqrt{\tau(t-\tau)}} d\tau - \int_0^t \frac{\operatorname{erf}\left(\frac{d}{4\sqrt{D_{H^+}(t-\tau)}}\right)}{\sqrt{\tau(t-\tau)}} d\tau \right)$$

$$= \frac{nFAC^*_{H_2O_2}}{2\pi}\sqrt{\frac{D_{H_2O_2}}{D_{H^+}}} \left(2\cdot\operatorname{asin}\left(\frac{t}{|t|}\right) - \int_0^t \frac{\operatorname{erf}\left(\frac{d}{4\sqrt{D_{H^+}(t-\tau)}}\right)}{\sqrt{\tau(t-\tau)}} d\tau \right)$$

$$c(t) = \frac{1}{2} nFAC^*_{H_2O_2}\sqrt{\frac{D_{H_2O_2}}{D_{H^+}}} \left[1 - \frac{1}{\pi}\int_0^t \frac{\operatorname{erf}\left(\frac{d}{4\sqrt{D_{H^+}(t-\tau)}}\right)}{\sqrt{(t-\tau)\tau}} d\tau \right] \qquad (5.7)$$

Equation (5.8):
Derivation of an expression for the delay time

For the delay time (the time between t = 0 and a significant concentration change at (x,y) = (0,0)) the slope of the response for small t is extrapolated (figure (5.4)). A straight line will be constructed through the point where the first derivative has the lowest variation.
Before the first derivative of (5.7) can be found, this equation must be simplified. The following series expansion is helpful:

$$\operatorname{erf}\left(\frac{L}{\sqrt{t-\tau}}\right)=\operatorname{erf}\left(\frac{L}{\sqrt{t}}\right)+\frac{L\cdot e^{-\frac{L^2}{t}}}{t^{\frac{3}{2}}\sqrt{\pi}}\cdot\tau+\frac{L\cdot e^{-\frac{L^2}{t}}}{t^{\frac{3}{2}}\sqrt{\pi}}\cdot\left(\frac{3}{4t}-\frac{L^2}{2t^2}\right)\cdot\tau^2+O\left(\tau^3\right)$$

with

$$L=\frac{d}{4\sqrt{D_{Red}}}. \qquad (5.9)$$

When $\sqrt{t} << L$ the series expansion can be reduced to:

$$\operatorname{erf}\left(\frac{L}{\sqrt{t-\tau}}\right)\approx\operatorname{erf}\left(\frac{L}{\sqrt{t}}\right).$$

This can be substituted in (5.7):

$$\begin{aligned}c(t)&\approx\frac{1}{2}nFAC^*_{Ox}\sqrt{\frac{D_{Ox}}{D_{Red}}}\left[1-\frac{1}{\pi}\int_0^t\frac{\operatorname{erf}\left(\frac{L}{\sqrt{t}}\right)}{\sqrt{(t-\tau)\tau}}d\tau\right]\\&=\frac{1}{2}nFAC^*_{Ox}\sqrt{\frac{D_{Ox}}{D_{Red}}}\left[1-\frac{1}{\pi}\operatorname{erf}\left(\frac{L}{\sqrt{t}}\right)\int_0^t\frac{1}{\sqrt{(t-\tau)\tau}}d\tau\right]\\&=\frac{1}{2}nFAC^*_{Ox}\sqrt{\frac{D_{Ox}}{D_{Red}}}\left[1-\frac{1}{\pi}\operatorname{erf}\left(\frac{L}{\sqrt{t}}\right)\cdot\pi\right]\\&=\frac{1}{2}nFAC^*_{Ox}\sqrt{\frac{D_{Ox}}{D_{Red}}}\left[1-\operatorname{erf}\left(\frac{L}{\sqrt{t}}\right)\right]\end{aligned}$$

The first and second derivatives become:

$$\frac{dc(t)}{dt} = -\frac{1}{2} nFAC^*_{Ox} \sqrt{\frac{D_{Ox}}{D_{Red}}} \left[\frac{4L}{\sqrt{\pi}} \frac{e^{-\frac{L^2}{t}}}{t^{\frac{3}{2}}} \right]$$

$$\frac{d^2c(t)}{dt^2} = -\frac{1}{2} nFAC^*_{Ox} \sqrt{\frac{D_{Ox}}{D_{Red}}} \left[\frac{4L}{\sqrt{\pi}} \left[\frac{L^2}{t} - \frac{3}{2} \right] \cdot \frac{e^{-\frac{L^2}{t}}}{t^{\frac{5}{2}}} \right]$$

so when

$$t_{max\ slope} = \frac{2}{3} L^2$$

the first derivative has it's maximum. The line through $v(t_{maxslope})$ with the slope as being calculated, crosses the time-axis at

$$t_{delay} = t_{max\ slope} - \frac{c(t_{max\ slope})}{\frac{d}{dt} c(t_{max\ slope})}$$

$$= \left(\frac{2}{3} + \left(\frac{2}{3} \right)^{\frac{3}{2}} \sqrt{\pi} \left[erf\left(\sqrt{\frac{3}{2}} \right) - 1 \right] e^{\frac{3}{2}} \right) \cdot L^2$$

$$\approx 0.307 \cdot L^2$$

Equation (5.10):
Derivation of the concentration for t ® ¥

From the series expansion:

$$\operatorname{erf}\left(\frac{L}{\sqrt{t-\tau}}\right)=\operatorname{erf}\left(\frac{L}{\sqrt{t}}\right)+\frac{L\cdot e^{-\frac{L^2}{t}}}{t^{\frac{3}{2}}\sqrt{\pi}}\cdot\tau+\frac{L\cdot e^{-\frac{L^2}{t}}}{t^{\frac{3}{2}}\sqrt{\pi}}\cdot\left(\frac{3}{4t}-\frac{L^2}{2t^2}\right)\cdot\tau^2+O\left(\tau^3\right)$$

it can be seen that the first term goes to zero for t ® ¥ (because erf(0)=0). All other terms contain a factor $\exp(-L^2/t)$, which goes faster to zero for t ® ¥ than any other t^x term, so

$$\lim_{t\to\infty}\operatorname{erf}\left(\frac{L}{\sqrt{t-\tau}}\right)=0$$

and so

$$\lim_{t\to\infty}\int_0^t\frac{\operatorname{erf}\left(\frac{L}{\sqrt{(t-\tau)}}\right)}{\sqrt{(t-\tau)\tau}}d\tau=0.$$

An expression for the final concentration is

$$C_{t\,inf}=\lim_{t\to\infty}c(t)=\frac{1}{2}nFAC^*_{H_2O_2}\sqrt{\frac{D_{H_2O_2}}{D_{H^+}}} \qquad (5.10)$$

References

[1] G. Jakobi and A. Löhr, Detergents and textile washing, principles and practice, VCH Verlagsgesellschaft mbH, Weinheim, Germany 1987

[2] M. Pourbaix, Atlas of electrochemical equilibria in aqueous solutions

[3] A.J. Bard and L.R. Faulkner, Electrochemical methods, fundamentals and applications, John Wiley & sons, Inc., New York, 1980

[4] H.S. Carslaw and J.C. Jeager,Operational methods in applied mathematics,Dover publications, Inc. New York, 1947

[5] M. Klein, Wasserhartebestimmung durch differenzmessung mit ISFETs, VDI Berichte, 1992, pages 127-131

Distribution list:

Prof.dr.ir. P. Bergveld (UT BIO)
Dr.ir. W. Olthuis (UT BIO)
A. Volanschi, M.Sc (UT BIO)
Dr.ir. R.J.R. Uhlhorn (URL)